Prediction of the effects of vortex shedding on UV disinfection efficiency

B. A. Younis and T. H. Yang

ABSTRACT

An assessment is made of the importance of vortex shedding which occurs from UV lamps on the efficacy of disinfection in UV channels. The focus is on the high Reynolds-number regime where turbulent flow conditions prevail and where there exists a strong interaction between the periodic mean-flow unsteadiness and the random turbulent motions. Simulations are performed of the flow around four circular lamps with axes perpendicular to the flow and which are arranged in a diamond configuration. Turbulence closure is achieved using a modified version of the $k-\varepsilon$ model which takes into account the modification of the turbulence energy spectrum due to vortex shedding. The disinfection efficiency is estimated using a Lagrangian approach in which the trajectories of massless particles are tracked to estimate their residence time and the dose received. The modified turbulence model shows that the occurrence of vortex shedding produces wide variation in the particles trajectories and, consequently, in the UV dose received. These and other results strongly suggest that the effects of vortex shedding on disinfection are very important and thus must be accounted for if the uncertainties inherent in the use of computational fluid dynamics (CFD) for the design of UV treatment channels are to be reduced.

Key words | CFD, disinfection, Lagrangian dose estimation, turbulence modeling, UV, vortex shedding

B. A. Younis (corresponding author)
T. H. Yang
Department of Civil & Environmental Engineering,
University of California – Davis,
Davis,
CA 95616,
USA
E-mail: *bayounis@ucdavis.edu*

INTRODUCTION

Recent years have seen significant increase in the use of computational fluid dynamics (CFD) in water-treatment applications (e.g. Lyn and Blatchley 2005; Elyasi and Taghipour 2006; Liu *et al*. 2007, Pan and Orava 2007). This has been prompted in part by the availability of CFD software packages that facilitate the rapid assessment of alternative designs. For the case of continuous flow UV channels, the availability of well-validated software provides a cost-effective tool for optimizing design parameters such as the number, spacing and power of UV lamps, and channel geometry required to achieve adequate disinfection of a given design flow rate. We are concerned here with a specific feature of flow in UV channels which is poorly handled by existing CFD software and which, we believe, introduces a significant element of uncertainty in the predictions. This feature is associated with the presence of vortex shedding which occurs when water, at various stages of disinfection, flows around vertical UV lamps. For Reynolds numbers greater than around 40 (based on cylinder diameter and average velocity), the flow around a lamp separates alternately from either side leading to the formation of regions of reversed flow (vortices) which proceed downstream forming a so-called Karman vortex street. The result is a fairly complex hydrodynamic field, which is very different from that found in a fully mixed, heterogeneous reactor. The question then arises as to the importance of vortex shedding in determining the UV dose delivered to the transported microorganisms and, consequently, the overall efficiency of the UV disinfection system. To our knowledge, this question has not been conclusively addressed. Thus, in the only previous study which specifically considered the effects of unsteadiness in the turbulent-flow regime (Lyn 2004), the effects of turbulence

doi: 10.2166/aqua.2011.008

were accounted for using the standard $k-\varepsilon$ turbulence closure. This is perhaps the most widely used turbulence model in CFD applications and hence its capabilities and limitations in a wide range of flows are well documented. It has conclusively been shown (e.g. Franke & Rodi 1993, Younis & Przulj 2006) that this model fails to yield accurate predictions of flows with vortex shedding. Specifically, the model seriously underestimates the strength of vortex shedding as exemplified, for example, by the root-mean-square of the velocity fluctuations. This unsatisfactory aspect of the standard $k-\varepsilon$ model arises because it does not account for the modification to the turbulence spectrum due to the interaction between the periodic large-scale mean-flow unsteadiness, and the random, small-scale turbulent motions. In disinfection channels, if the extent of the vortex shedding process is incorrectly predicted then so also will be the microorganisms' residence time in a UV field of given intensity and, consequently, the received dose. This is then the objective of this work: to obtain accurate predictions of the vortex shedding process from a cluster of UV lamps, and use the results to quantify the importance of vortex shedding on the efficacy of disinfection. To achieve this objective, we incorporate into a two-dimensional finite-volume CFD solver a modification to the $k-\varepsilon$ model to handle vortex shedding, and verify the outcome by comparisons with experimental data. The solver is then extended to calculate the UV dose using a Lagrangian approach. Calculation of the particles' residence time and of the UV intensity field enables estimation of the UV dose and thereafter the efficiency of disinfection. Comparisons between results obtained with and without the model modification provide the basis for conclusions regarding the importance of vortex shedding to the disinfection process.

MATHEMATICAL MODEL

Mean-flow equations

The equations of conservation of mass and momentum for a constant density fluid are:

$$\frac{\partial U_i}{\partial x_i} = 0 \tag{1}$$

$$\frac{\partial U_i}{\partial t} + U_j \frac{\partial U_i}{\partial x_j} = \frac{\partial}{\partial x_j}\left(\nu \frac{\partial U_i}{\partial x_j} - \overline{u_i' u_j'}\right) - \frac{1}{\rho}\frac{\partial P}{\partial x_i} \tag{2}$$

In the above, U_i is the time-averaged velocity vector, P is the static pressure and ρ and ν are, respectively, the water's density and kinematic viscosity. For compactness, the conventional Cartesian-tensor notation is employed wherein the repeated indices imply summation.

In the flows under consideration, the Reynolds number is sufficiently high for it to be impractical to simulate the behavior of the flow by solving the conservation equations for the instantaneous flow variables (Pope 2000). Instead, the equations are averaged over a time interval Δt:

$$\overline{\varphi} = \frac{1}{\Delta t}\int_t^{t+\Delta t} \hat{\varphi}\,\mathrm{d}t \tag{3}$$

where $\hat{\varphi}$ signifies an instantaneous value. In this study, Δt is taken to be the same as the *computational* time step. This implies that fluid motions having time scales greater than Δt (e.g. the large-scale vortices that are shed from around the UV lamps) are captured directly in the computations while motions occurring at time scales smaller than the computational time step (e.g. the turbulent motions) are filtered out and their effects on the transport of mass, momentum and microorganisms will need to be taken into account via a suitable turbulence closure. This averaging process is quite distinct from the conventional 'Reynolds averaging' wherein $\Delta t \to \infty$ and which is therefore appropriate only to steady flows. It is also distinct from 'ensemble averaging' which requires the period of the oscillations to be known *a priori*. The only requirement that needs to be met for the present averaging to be valid is that the computational time step should be significantly greater than the time scale associated with the turbulent fluctuations. This is clearly the case in the present applications where the mean-flow Reynolds number (based on bulk channel velocity and cylinder diameter) is of the order of 6000. Irrespective of the way in which the averaging process is interpreted, the final outcome is the same: namely the appearance in the averaged momentum equations of the Reynolds stresses which are unknown and which will first need to be determined before the equations may be solved.

The turbulence model

The unknown Reynolds stresses ($-\rho\overline{u_i'u_j'}$) are modeled using an eddy-viscosity closure based on Boussinesq's assumption of linear stress-strain relationship:

$$-\rho\overline{u_i'u_j'} = \mu_t\left(\frac{\partial U_i}{\partial x_j}+\frac{\partial U_j}{\partial x_i}\right)-\frac{2}{3}\rho\delta_{ij}k \tag{4}$$

The eddy viscosity (μ_t) is defined in terms of two turbulence parameters: the turbulence kinetic energy (k) and its rate of dissipation by viscous action (ε):

$$\mu_t = C_\mu\rho\frac{k^2}{\varepsilon} \tag{5}$$

k and ε are determined from the solution of the differential transport equations:

$$\frac{\partial k}{\partial t}+U_j\frac{\partial k}{\partial x_j}=\frac{\partial}{\partial x_j}\left(\frac{\nu_t}{\sigma_k}\frac{\partial k}{\partial x_j}\right)+P_k-\varepsilon \tag{6}$$

$$\frac{\partial \varepsilon}{\partial t}+U_j\frac{\partial \varepsilon}{\partial x_j}=\frac{\partial}{\partial x_j}\left(\frac{\nu_t}{\sigma_\varepsilon}\frac{\partial \varepsilon}{\partial x_j}\right)+C_{\varepsilon 1}\frac{\varepsilon}{k}P_k-C_{\varepsilon 2}\frac{\varepsilon^2}{k} \tag{7}$$

where P_k is the rate of production of turbulence kinetic energy:

$$P_k = -\overline{u_i'u_j'}\frac{\partial U_i}{\partial x_j}. \tag{8}$$

The model coefficients are assigned their usual values (Launder and Spalding 1972).

It has already been mentioned that the $k-\varepsilon$ model, in its standard form, yields incorrect prediction of vortex shedding due to its inability to account for the modification of the spectral transfer process brought about by the presence of vortex shedding. In steady flows, the rate at which energy enters the turbulent motion at the large scales is equal to the rate at which energy is dissipated by viscosity at the smallest scales. When vortex shedding is present, experiments show that there occurs direct energy input into the spectrum at a frequency which corresponds exactly to the vortex-shedding frequency. This discrete input produces a lag in between the generation of turbulence energy at the large scale and its dissipation at small scales. This phenomenon was discussed in detail in Younis & Zhou (2006) who proposed a modification to the equation for ε which takes this lag into account. This modification enters the ε equation via the "production of dissipation" term and amounts to redefining the coefficient $C_{\varepsilon 1}$ thus:

$$C_{\varepsilon 1} = C_{\varepsilon 1}\left(1+C_t\frac{k}{\varepsilon}\frac{1}{Q+k}\left|\frac{\partial(Q+k)}{\partial t}\right|\right) \tag{9}$$

where $Q = 1/2(U^2+V^2)$ is the mean-flow kinetic energy and C_t is a coefficient assigned the value of 0.38 by numerical optimization.

The model for UV inactivation

The UV dose received by the microorganisms was estimated using a Lagrangian approach wherein the microorganisms are treated as massless particles. These particles are introduced into the flow at the channel inlet and at specified intervals in time and their trajectories are tracked through the flow field. The dose received by each microorganism is determined by its local velocity, its trajectory and by the intensity of the UV field along its route. As the particles' trajectory is greatly influenced by the strength of the vortex shedding from the UV lamps, this approach presents a simple yet effective way to assess the importance of this phenomenon in determining the disinfection efficiency.

The trajectory of a massless particle is determined from integration of the local velocity vector over a suitable time interval:

$$\vec{r} = \vec{r}_0+\int_0^t \vec{V}\,\mathrm{d}t \tag{10}$$

where $\vec{r}_0$ is the particle position at time $t=0$ and $\vec{V}$ is the two-dimensional unsteady local velocity obtained from the solution of Equations (1)–(9).

In evaluating Equation (10), the interval of integration is taken to be the same as the computational time step while the velocity is taken as the average of the values at the initial and final positions. Since the final velocity depends on the yet to be determined position, a number of iterations were performed to arrive at a converged solution.

The particles were released at the channel inlet, at a uniform rate, and at uniform spacing Δs in the vertical direction:

$$\Delta s = \frac{B}{n} \tag{11}$$

where n is the number of released particles and B is the distance over which the particles are released. In the results presented below, this distance was set equal to $\pm 3D$ from the centerline (i.e. the plane $y/D = 0$) where D is the diameter of a UV lamp. As the flow field around the lamps was dominated by the unsteady shedding of vortices, particles were continually released from these locations in order to fully represent the time-varied trajectories.

Regarding the estimation of the UV intensity (I_i) at each point within the disinfection channel, several models exist and a complete review can be found in Liu *et al.* (2004). The model adopted here is the point source summation in the form suggested by Lyn *et al.* (1999). This model does not account for the 'shadow' effects but incorporates the effects of absorption by the quartz tubing and the fluid continuum. In this model, the UV intensity at a point with coordinates (x, y) due to a single UV lamp is obtained from:

$$I_i = \frac{S}{L}\int_{-L/2}^{L/2} \frac{1}{4\pi(r^2+z^2)} \times \exp\left\{\left\{-\left[\alpha_W(1-D/2r)+\alpha_q(t/r)\right](r^2+z^2)^{1/2}\right\}\right\}\mathrm{d}z \tag{12}$$

where S = total power output of the single lamp, L = total length of a lamp placed at (x_i, y_i) in the channel, $r^2 = (x-x_i)^2 + (y-y_i)^2$, z = vertical coordinate, α_w and α_q are absorption coefficients of radiation in water and in quartz tubing and t =thickness of the quartz jacket. When a number (N) of lamps is present, the resulting UV intensity at a point $I(x, y)$ in the flow field is simply the sum of contributions from all the lamps, i.e.

$$I(x,y) = \sum_{i=1}^{N} I_i(x,y;x_i,y_i) \tag{13}$$

Once the UV intensity field in the channel was determined from Equation (13) then that, together with knowledge of the position of each released particle, combine to provide estimate of the dose (D_j) which is accumulated by each microorganism as it flows through the entire channel's length. This dose is obtained from:

$$D_j = \int_0^{t_P} I\mathrm{d}t = \sum I_i \Delta t_P \tag{14}$$

where t_p is the total particle travel time in the channel and Δt_p is the time step used to track the trajectory of the particle.

Disinfection efficiency

The number of microorganisms that remain viable (N_j) is estimated by the first-order Chick-Watson inactivation kinetics model (e.g. Loge *et al.* 1996, Lyn 2004):

$$N_j = e^{-KD_j}N_0 \tag{15}$$

where N_0 represents the number of microorganisms released at channel's inlet and $K = 0.59\ \mathrm{cm}^2/(\mathrm{mWs})$ represents the inactivation rate constant (Lyn *et al.* 1999). The extent of disinfection is then calculated from:

$$\overline{N} = \frac{1}{n_{exit}}\sum_{j=1}^{n_{exit}}\frac{N_j}{N_0} = \frac{1}{n_{exit}}\sum_{i=1}^{n_{exit}} e^{-KD_i} \tag{16}$$

in which $\overline{N}$ is the average extent of disinfection at the channel outlet and n_{exit} is the total number of particles exiting the channel.

The computational model

The above equations were solved using the finite-volume methodology described in Demirdzic *et al.* (1997). Discretization in both space and time was second-order accurate. The solution algorithm was iterative and utilized the SIMPLE algorithm to ensure that the continuity and momentum equations were simultaneously satisfied at each time step. Convergence was considered to have been achieved when the sum of the absolute normalized residuals for all dependent variables fell below 10^{-3}. Once a periodic

solution was attained, this level of convergence was typically attained in three iterations.

To improve the numerical accuracy of the computed results, the time-step size was set equal to a value smaller than the local convective and viscous time scales. The Courant-Friedrichs-Lewy (CFL) stability condition was enforced using the smallest grid spacing (Δh) which is obtained in the part of the grid adjacent to the wall surface of each cylinder. With this, the CFL condition places an upper limit on the time-step size, specifically $\Delta t^* < (1/2)(\Delta h/D)$ where Δt^* is the non-dimensional time-step size defined $\Delta t^* = (U_0 t/D)$. For the test flow considered in the next section, this constraint produced a physical time-step size $\Delta t = 0.00036$s ($\Delta t^* = 0.0034$).

RESULTS AND DISCUSSION

To check the performance of the computational model, simulations were performed for the turbulent flow around a single square-sectioned cylinder at Reynolds number (Re) = 20,000. This is a case for which results from experiments and other simulations are available. Of interest is the models' ability to capture the correct magnitude of the fluctuating lift and drag forces that act on the cylinder. Figure 1 shows these forces presented in non-dimensional form as the lift and drag coefficients C_L and C_D. The standard k – ε model was applied up to the non-dimensional time $t^* = 550$. Thereafter, the modified model was used. The predicted average value of C_D is higher with the modified model. This indicates that the time-averaged size of the region of reversed flow which develops behind the cylinder is larger in extent than that predicted by the standard model. Consequently, the two models' results for particle trajectories will be quite different. The fluctuations in C_D are also increased. The time-averaged value of the lift coefficient is zero irrespective of the model used. This is to be expected since the cylinder geometry and the boundary conditions are symmetric. The enhanced fluctuations obtained with the modified model are perhaps the most important feature of the modified model's performance.

The vortex shedding frequency f is presented in non-dimensional form as the Strouhal number $S_t = fD/U_0$,

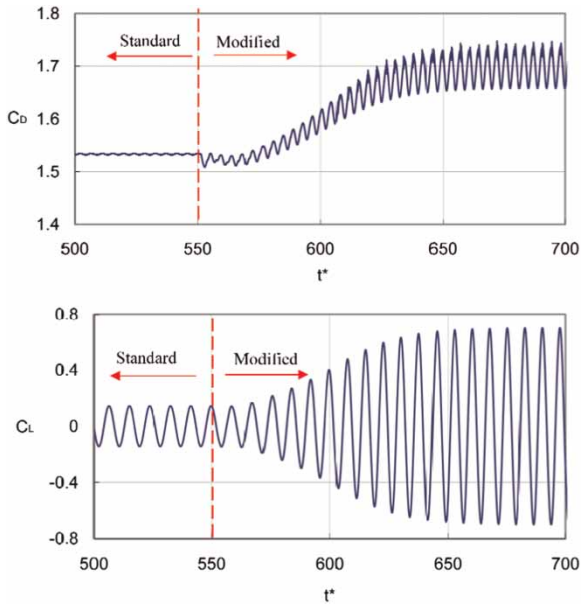

Figure 1 | Predicted drag- (top) and lift-coefficients for single square cylinder as obtained with the standard and the modified models.

where D is the diameter and U_0 is the average velocity. To determine f, a fast-Fourier transform (FFT) was performed on the time-series of the lift coefficient to identify the dominant frequency of fluctuation. A quantitative measure of the strength of vortex shedding is obtained by evaluating the root-mean-square (r.m.s.) values of the lift and drag coefficients C_L' and C_D' – parameters that provide a sensitive indication of the intensity of the vortex shedding. The results are presented in Table 1. The most striking result there is the enormous difference between the r.m.s. values obtained with the standard and the modified versions of the k – ε

Table 1 | Predicted and measured vortex-shedding parameters

Source	S_t	$\overline{C_D}$	C_D'	C_L'
Numerical predictions				
Modified k – ε model	0.133	1.788	0.027	0.819
Standard k – ε model	0.117	1.533	0.0009	0.102
LES* (Wang & Vanda 1996)	0.13	2.03	0.18	0.04
Experimental data				
Bearman *et al.* (1982)	0.13	–	–	1.20
Lyn (1995)	0.132	2.1	–	–

*LES: large-eddy simulations.

model. Note, in particular, the negligibly small values obtained for the r.m.s. of the drag coefficient with the standard model.

Attention is now turned to the benchmark flow used here to illustrate the effects of vortex shedding on UV disinfection. The configuration of the disinfection channel considered is shown in Figure 2. This configuration is similar to that studied computationally by Lyn *et al.* (1999) and Lyn & Blatchley (2005) and experimentally by Chiu (1999). The actual flow domain simulated here is defined in Figure 2(a). All the lamps are located within quartz sleeves that have a diameter $D = 0.025$ m. The extent of the solution domain was chosen in such a way as to ensure that the results were independent of the domain size. Only two-dimensional simulations were performed; the computational domain shown being a plane perpendicular to the lamps and passing through their middle. The UV intensity model Equation (13) was used to compute the UV intensity on this center plane. Thus the contributions to the total intensity on the center plane due to the lamp lengths on either side of it were included in the computations.

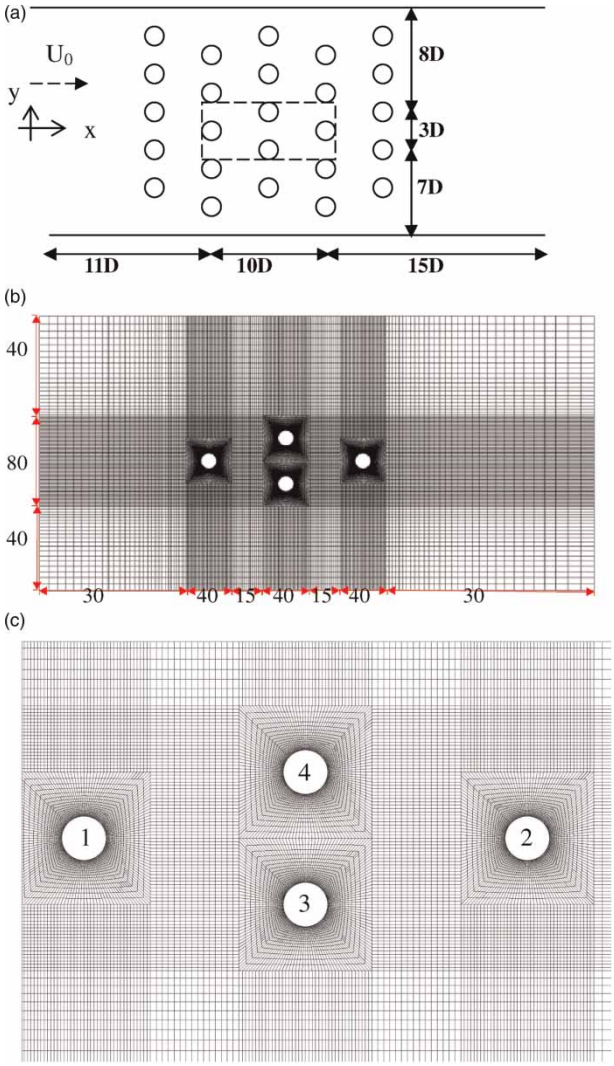

Figure 2 | Computational domain and details of grid used. (a) configuration of UV disinfection channel and extent of computational domain, (b) numerical grid, (c) grid arrangement near tubes.

The boundary conditions used were as follows: at inlet to the solution domain, a uniform velocity distribution was specified with the velocity assigned a value $U_0 = 0.24$ m/s which gives Re $= U_0 D/\nu = 6000$. This value is the same as that used in the experiments of Chiu (1999) and the simulations of Lyn *et al.* (1999) and Lyn & Blatchley (2005). The profiles of turbulence kinetic energy and dissipation were obtained from the assumption that the turbulence was isotropic with a relative turbulent intensity ($=u'/U$) of 0.02 and a turbulence length scale of 0.019. At the outlet, the flow was assumed to be fully developed and thus a zero streamwise gradient was specified for all the dependent variables. On the surface of each lamp, the flow was assumed to be fully turbulent and to obey the universal logarithmic law of the wall (Launder & Spalding 1972). The upper and lower boundaries were assumed to be planes of symmetry. The numerical accuracy of the results were checked by performing the calculations on several grids and time-step sizes. The results presented below were obtained with a grid consisting of 44,400 active nodes non-uniformly distributed with the greater concentration being in the vicinity of the lamps. Each lamp had 160 nodes in direct contact with it. Systematic grid-dependence checks were performed and the results presented herein are sensibly free of grid effects.

An overall view of the flow which occurs around this configuration can be seen in Figure 3. Plotted there are the instantaneous contours of turbulent viscosity obtained

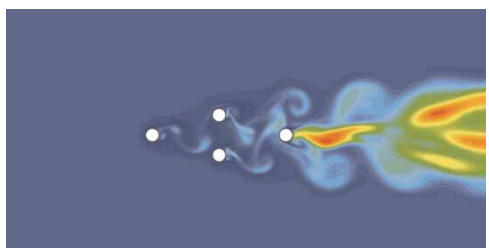

Figure 3 | Predicted contours of turbulent viscosity with modified model.

with the modified model. The resulting flow behavior is quite complex, being characterized by strong interactions between the unsteady wakes produced by the various lamps. The results of these interactions are quantified by the parameters presented in Table 2. The frequencies in that table were obtained by performing FFT analysis on a time series consisting of 2^{12} data points. Immediately apparent are the higher values of the r.m.s. fluctuations which are captured by the modified model on all lamps. For the upstream lamp (lamp number 1 in Figure 2), the average drag coefficient is predicted to be nearly 1.2, which is close to the experimentally found value for an isolated circular cylinder. In contrast, lamp 2, which is effectively shielded by the lamp upstream of it, experiences a drastically reduced value of the drag coefficient. Lamps 3 and 4 experience the same average lift and drag forces with the lift forces acting upon them being exactly out of phase.

In calculating the UV intensity using Equation (12), the parameters that appear there were assigned the same values as those used by Chiu (1999), Lyn (2005) and Lyn *et al.* (1999) namely: the power output of a single lamp S = 26.7W; the length of each lamp L = 147 cm; the absorption coefficients of radiation in water $\alpha_w = 0.44\ \text{cm}^{-1}$ and in quartz tubing $\alpha_q = 0.63\ \text{cm}^{-1}$ and the thickness of the quartz jacket $t = 0.15$ cm. The contribution from the out-of-plane parts of each UV lamp was obtained by sub-dividing the vertical length into 1000 segments and then by incorporating the intensity due to each segment into Equation (12). The resulting UV intensity field using 200 segments is shown in Figure 4. The maximum intensity level obtained was 29 mW/cm^2, which is identical to the value obtained by Chiu (1999).

In the simulations that follow, the massless particles were released at the channel inlet and at equidistant vertical intervals spanning the distance from the centerline ($y/D = 0$) to $y/D = \pm 3$. The particles were continuously released throughout the vortex-shedding cycle. The accuracy of the dose estimates depends strongly on the number of particles tracked. Thus, too few particles will inevitably lead to deterioration in the reliability of method (Munoz *et al.* 2007). On the other hand, the tracking of too many particles will pose serious logistical problems in terms of computer resources. In this work, and in order to gauge the extent to which the results depend on the number of particle released, we performed the statistical analysis using two sample sizes: 1000, 2000. To demonstrate the sensitivity of the results to the number of samples, simulations were also obtained with the unrealistically small sample size of 13 (this number being arrived at by releasing six particles on either side of the center plane, and one at the center itself). The results, presented as the distribution of received dose distribution as obtained by each sample, are shown in Figure 5 where it can be seen that the predictions of 1000 and 2000 particles are very closely matched, with the maximum difference within any particular interval being no more than 1%. The same result is expressed quantitatively in Table 3 where the extent of disinfection (-log(N/N_0)) and the reduction equivalent dose (RED) predicted by each release are presented. The RED is defined as the UV dose derived by entering the log inactivation measured during full-scale reactor testing into the UV dose-response curve that was derived through collimated beam testing. The RED values are specific to the microorganism used during experimental testing and the validation test conditions for full-scale reactor testing. Table 3 also shows the RED values obtained using three alternative inactivation

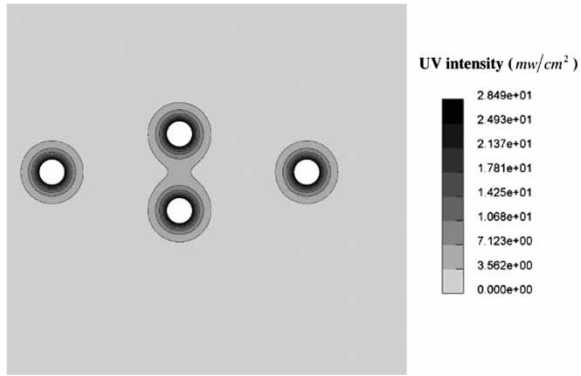

Figure 4 | Simulated UV intensity field by point source summation.

Table 2 | Predicted Strouhal number and force coefficients for lamps 1–4

Turbulence model	Lamp number	S_t	$\overline{C_D}$	C'_D	$\overline{C_L}$	C'_L
Standard $k-\varepsilon$	1	0.159	0.75	0.030	0.0034	0.0194
	2	0.159	0.60	0.042	0.0020	0.0346
	3	0.159	0.88	0.026	0.0308	0.0248
	4	0.159	0.87	0.026	0.0267	0.0238
Modified $k-\varepsilon$	1	0.194	1.19	0.116	0.023	0.805
	2	0.194	0.38	0.088	0.014	0.656
	3	0.194	1.24	0.236	-0.408	1.098
	4	0.194	1.21	0.234	0.408	1.091

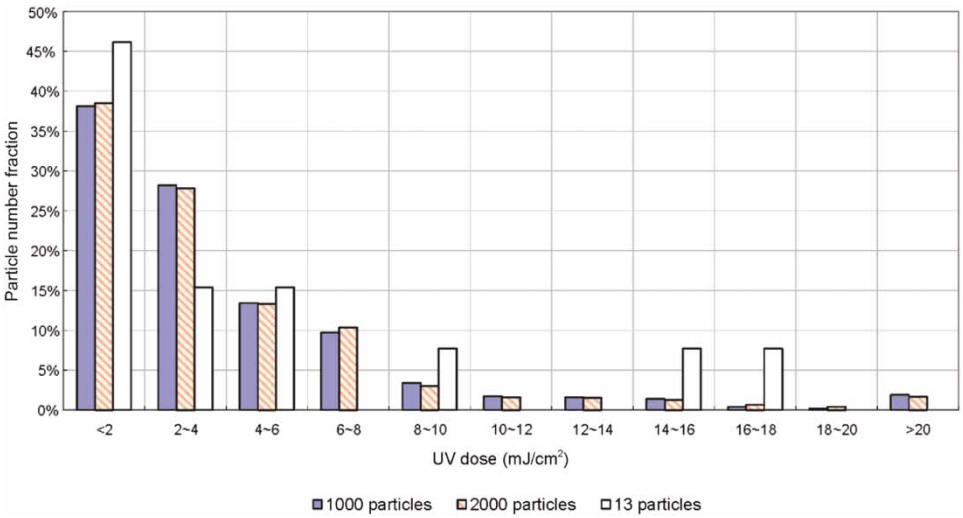

Figure 5 | Comparisons of dose-distribution from different number of released particles.

Table 3 | Predictions of extent of disinfection and reduction equivalent dose using different number of particles and different inactivation mechanisms

		RED (mJ/cm^2)		
Number of particles	**Extent of disinfection (−log(N/N_0))**	**Lyn *et al.* (1999)**	**Liu *et al.* (2007)**	**Munoz *et al.* (2007)**
1000	0.509	1.99	2.99	3.94
2000	0.509	1.99	2.99	3.94
13	0.460	1.85	2.93	3.76

equations namely those proposed by Lyn *et al.* (1999), Liu *et al.* (2007), and Munoz *et al.* (2007). The discrepancies between the different models results are not negligible but what is relevant here is the fact that, irrespective of which inactivation equation is used, the results obtained by tracking 1000 particles are essentially identical to those obtained with 2000 particles.

Turning now to consideration of the effects of vortex shedding on disinfection, the predicted particle trajectories are expected to depend strongly on the choice of the turbulence model used. Figure 6 shows the particles trajectories predicted using both the standard and the modified $k-\varepsilon$ models. The most striking feature of the trajectories as predicted by the standard model is their very small departures from the patterns that would be expected in steady-state flows. This is not surprising in view of this model's known inability to capture vortex shedding of appropriate intensity.

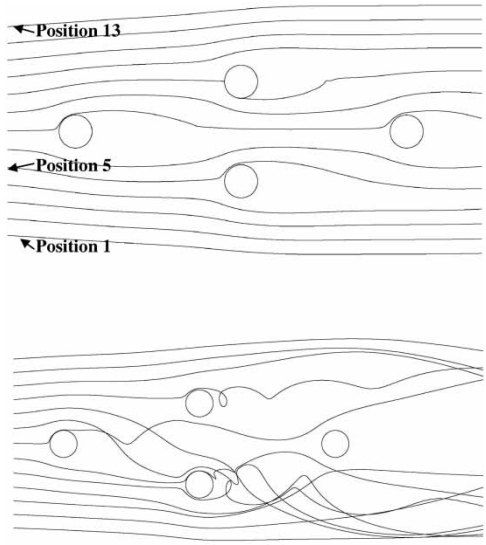

Figure 6 | Comparisons of predicted particle trajectories. Standard $k-\varepsilon$ model (top), modified $k-\varepsilon$ model (bottom).

There is no evidence of particles being entrained by the coherent structures, or of them being deflected by the strong shear that is set up in the cross-flow direction. This is in sharp contrast with the results obtained using the modified $k-\varepsilon$ model, shown in the same figure. Here, the significant deflection experienced by some particles is quite apparent most notably by a particle release from above the center plane which is then entrained by the wake of the leading lamp and is deflect to a location well

below this plane. The 'detention' of some particles in the reversed flow regions is also quite apparent as evidenced by their looped trajectories.

Comparisons of the residence time of the particles released at $t^* = 0$ as predicted by the standard and the modified model are shown in Figure 7. In that figure, the particles' release position, which is plotted on the horizontal axis, refers to the location of the release with respect to the centerline, Thus, for example, position 1 indicates a particle released at location $y/D = -3$, while position 13 refers to the location $y/D = +3$. The effects of vortex shedding are seen to generally increase the particles residence time in the channel. In Figure 8, the UV dose received by the particles is plotted against the release position. This quantity turns out to be only approximately proportional to the particle residence time. This is especially true for the modified model as can be seen, for example, from this model's results for the particles released from positions 5 and 8. While the residence times associated with these two positions are virtually the same, the received doses for particles released from the same positions differ by a factor of nearly 2. The implication of these findings is that particles receive a high UV dose because their trajectories, which are largely affected by the organized vortex shedding from the tubes, bring them into regions of high UV intensity, even though their total residence time within the channel is relatively short. Moreover, particles released at the same position but at different time also receive different UV dose due to the

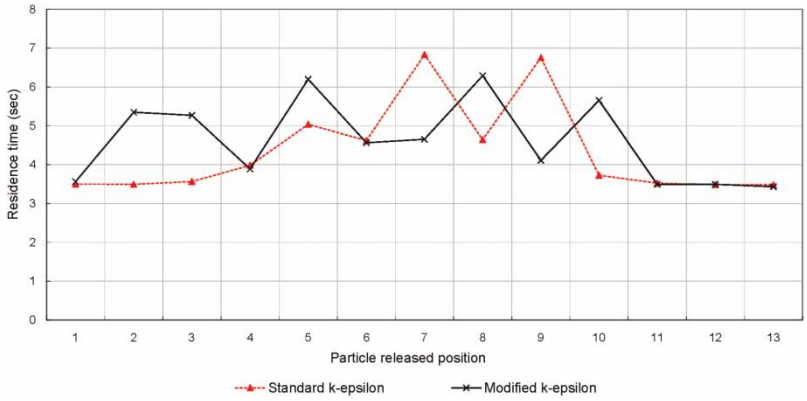

Figure 7 | Prediction of particle residence time with different turbulence models.

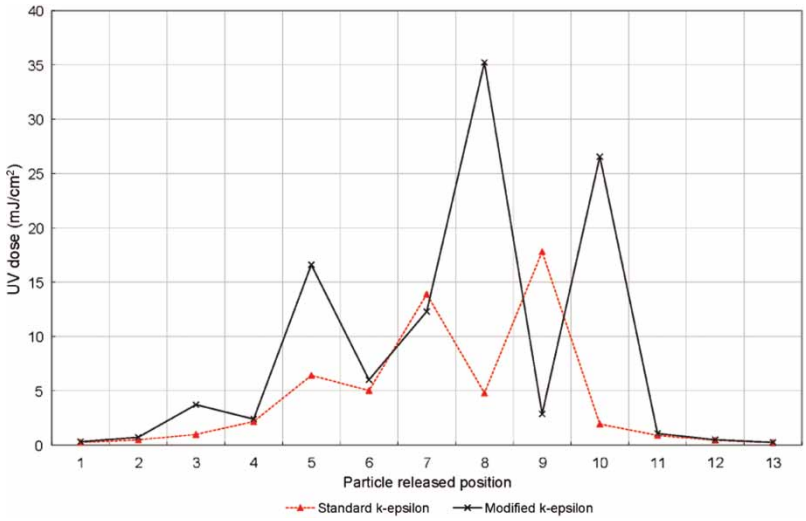

Figure 8 | Prediction of UV dose received by particles released at $t^* = 0$ with different turbulence models.

large-scale deflections associated with vortex shedding. The consequences on the total residence time are to make this parameter strongly dependent on the location of the particle release. As a result, the UV dose received will also depend strongly on the phase at which the particle was released in the channel. Figure 9 confirms this and shows that particles that enter the channel from exactly the same location, but at different phases of the vortex-shedding cycle, can receive doses that are different by a factor of 7.

The sensitivity of the calculated extent of disinfection to vortex shedding can be seen in Figure 10 which compares the dose distribution as predicted with the standard and the modified models. The modified $k-\varepsilon$ model results show that the fraction of particles receiving a certain UV dose decreases monotonically with increase in dose thereby producing a distribution which has a single peak. In contrast, the standard model results show that there exist two peaks in the fraction-dose distribution – a result which suggests that this model will produce an overestimation of the extent of disinfection that can be obtained in a particular channel.

Although the entry of the untreated water to the disinfection channel is continuous, it is nevertheless instructive to examine the effects of phase at the time of entry on the UV dose received by the microorganisms. It would be reasonable to expect that the strongly time-dependent nature of the flow will mean that microorganisms introduced at certain phases of the shedding cycle may receive a dose below the safe limit, even though the cycle-averaged dose is within these limits. In Figure 11, the dose distributions received by particles introduced at four different phases of the shedding cycle are compared. The results clearly demonstrate that the UV dose received by microorganisms and, consequently, their extent of disinfection will depend on the phase at which they enter into the disinfection channel.

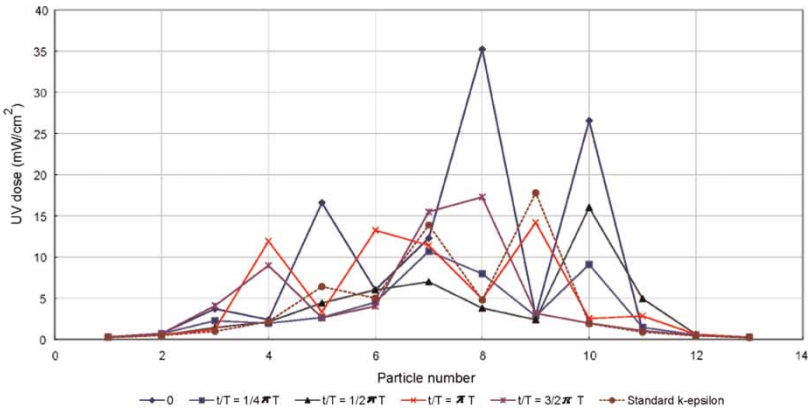

Figure 9 | Dependence of received dose on position of particle release.

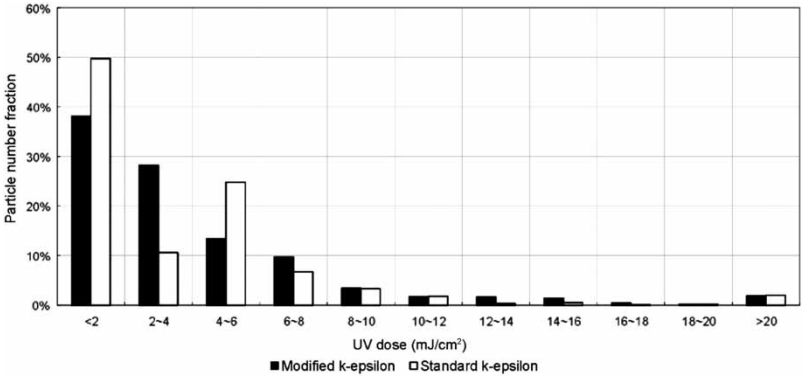

Figure 10 | Comparison of dose-distribution as predicted by the standard and the modified models.

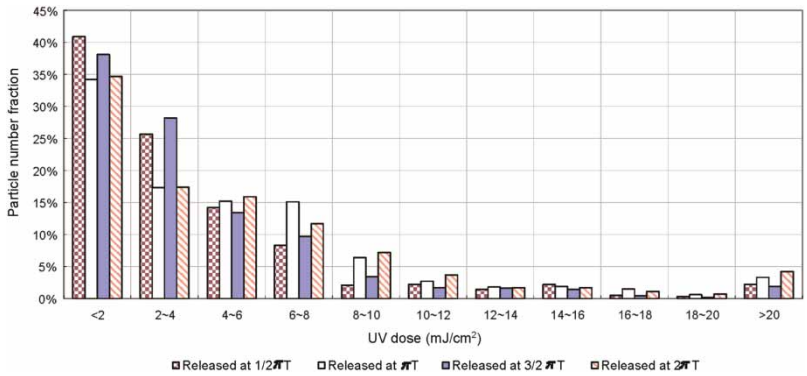

Figure 11 | Comparisons of dose-distributions as a function of release phase.

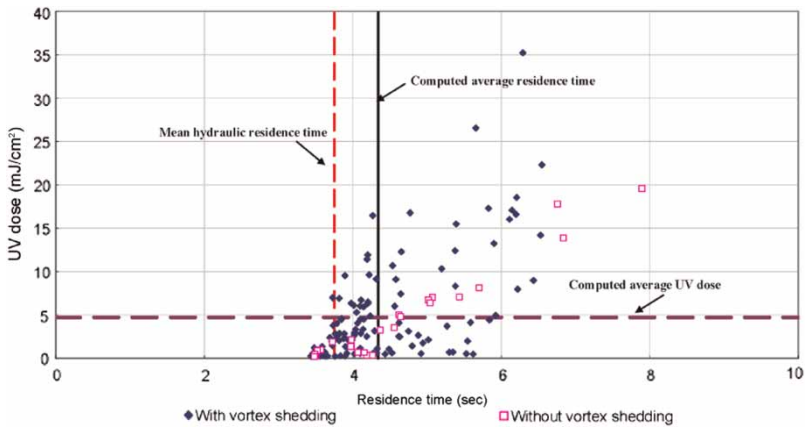

Figure 12 | Received UV dose versus residence time: regime analysis.

A final demonstration of the need to accurately predict vortex shedding in the design of UV disinfection channels is provided in Figure 12 where the predicted results are presented in the form of four regimes formed by the intersection of the lines of average residence time and average received dose. Theses averages were obtained by averaging the residence time and the received dose for all released particles over the entire period of the simulations. In the figure, the four regimes correspond to low UV dose, low residence time (I), low UV dose, high residence time (II), high UV dose, low residence time (III), and high UV dose, high residence time (IV). To maximize hydrodynamic efficiency while maintaining a safe disinfection performance, operations in regime III are desired since there the UV dose is higher than the average value while the residence time is kept to a minimum. It would also be acceptable for the disinfection channel to be operated in conditions of regime IV but, clearly, not in regimes I and II since the received UV dose will then fall below the acceptable minimum. Compared with the weak vortex-shedding results, the proportion of particles located in regions III and IV is higher when vortex shedding is correctly captured in the simulations. An almost linear relationship between UV dose and residence time is obtained when vortex shedding is absent due largely to the undisturbed or steady particle trajectories. By using the modified model, the trajectories are strongly influenced by the vortex shedding with important implications on their actual residence time in the disinfection channel. The mean hydraulic residence time (defined as L/U_0 where L is the tank length and U_0 is the inlet velocity) is also shown in Figure 12. The results show that the average residence time, which is computed taking into account the vortex shedding, is longer than the mean hydraulic residence time. This result indicates that if the effects of vortex shedding are not correctly predicted then the particle residence time will be underestimated leading to the possibility of arriving at overly conservative designs.

CONCLUSIONS

To assess the importance of vortex shedding on the disinfection efficiency, computations were obtained for the flow around four UV lamps arranged in diamond formation using a modified form of the widely used $k-\varepsilon$ model of turbulence. Previous computations have all used the standard form of this model which is known to fail in producing the correct intensity of the vortex shedding. The results obtained show that the modified model succeeds in capturing the complex flow field produced from interaction between the vortices shed from each of the UV lamps and the lamps themselves. Application of Lagrangian methodology to determine the trajectories of massless particles and estimate the UV dose they receive showed that significant differences can result depending on whether or not the simulations succeed in capturing the occurrence and intensity of vortex shedding. These results suggest that the uncertainty associated with the use of CFD in the design of UV disinfection channels can be reduced through properly accounting for the effects of vortex shedding. The principal contributions of this work are thus in highlighting the importance of this phenomenon, and in presenting a simple way in which the performance of a widely used turbulence model can be improved.

REFERENCES

Bearman, P. W. & Obasaju, E. D. 1982 An experimental study of pressure fluctuations on fixed and oscillating square-section cylinders. *J. Fluid Mech.* **119**, 297–321.

Chiu, K., Lyn, D. A., Savoye, P. & Blatchley III, E. R. 1999 Integrated UV disinfection model based on particle tracking. *J. Environ. Engineer.* **125**(1), 7–16.

Demirdzic, I., Muzaferija, S. & Peric, M. 1997 Advances in computation of heat transfer, fluid flow and solid-body deformation using finite-volume approaches. In: *Advances in Numerical Heat Transfer* (Ed. W. Minkowycz & E. M. Sparrow), pp. 59–96.

Elyasi, S. & Taghipour, F. 2006 Simulation of UV photoreactor for water disinfection in Eulerian framework. *Chem. Engineer. Sci.* **61,** 4741–4749.

Franke, R. & Rodi, W. 1993 Calculation of vortex shedding past a square cylinder with various turbulence models. In: *Turbulent Shear Flows 8*, (Ed. F. Durst *et al.*), Springer, New York, pp. 189–204.

Launder, B. E. & Spalding, D. B. 1972 *Mathematical Models of Turbulence.* Academic Press, New York.

Liu, D., Ducoste, J., Jin, S. & Linden, K. 2004 Evaluation of alternative fluence rate distribution models. *J. Water SRT – Aqua* **53**(6), 391–408.

Liu, D., Wu, C., Linden, K. & Ducoste, J. 2007 Numerical simulation of UV disinfection reactors: Evaluation of alternative turbulence models. *Appl. Math. Model.* **31**, 1753–1769.

Loge, F. J., Emerick, R. W., Heath, M., Jacangelo, J., Tchobaboglous, G. & Darby, J. L. 1996 Ultraviolet disinfection of secondary wastewater effluents: prediction of performance and design. *Water Environ. Res.* **68**, 900.

Lyn, D. A. 2004 Steady and unsteady simulations of turbulent flow and transport in ultraviolet disinfection channels. *J. Hydraul. Engineer.* **130**(9), 762–770.

Lyn, D. A. 1995 A laser-Doppler velocimetry study of ensemble-averaged characteristics of the turbulent near wake of a square cylinder. *J. Fluid Mech.* **304**, 285–319.

Lyn, D. A. & Blatchley III, E. R. 2005 Numerical computational fluid dynamics-based models of ultraviolet disinfection channels. *J. Environ. Engineer.* **131**(6), 838–849.

Lyn, D. A., Chiu, K. & Blatchley III, E. R. 1999 Numerical modeling of flow and disinfection in UV disinfection channels. *J. Environ. Engineer.* **125**(1), 17–26.

Munoz, A., Craik, S. & Kresta, S. 2007 Computational fluid dynamics for predicting performance of ultraviolet disinfection-sensitivity to practice tracking inputs. *J. Environ. Engineer. Sci.* **6**, 285–301.

Pan, H. & Orava, M. 2007 Performance evaluation of the UV disinfection reactors by CFD and fluence simulations using a concept of disinfection efficiency. *J. Water SRT – Aqua* **56**(3), 181–189.

Pope, S. B. 2000 *Turbulent Flows*. Cambridge University Press, Cambridge.

Younis, B. A. & Przulj, V. 2006 Computation of turbulent vortex shedding. *Computational Mechanics* **37**(5), 408–425.

Younis, B. A. & Zhou, Y. 2006 Accounting for mean-flow periodicity in turbulence closures. *Phys. Fluids* **18**(1), doi: 10.1063/1.2166458.

Wang, G. & Vanda, S. P. 1996 *Large-eddy simulations of high Reynolds number turbulent flow over a square cylinder*. Rep. III (2)/1996, Dept. of Mech. and Ind. Engg., University of Illinois Urbana-Champaign.

First received 22 February 2010; accepted in revised form 29 September 2010